


# Influence of mechanically-induced dilatation on the shape memory behavior of amorphous polymers at large deformation

Drew W. Hanzon<sup>1</sup> · Haibao Lu<sup>2</sup> ·  
Christopher M. Yakacki<sup>1</sup> · Kai Yu<sup>1</sup> 

Received: 6 August 2017 / Accepted: 13 January 2018 / Published online: 22 January 2018  
© Springer Science+Business Media B.V., part of Springer Nature 2018

**Abstract** In this study, we explore the influence of mechanically-induced dilatation on the thermomechanical and shape memory behavior of amorphous shape memory polymers (SMPs) at large deformation. The uniaxial tension, glass transition, stress relaxation and free recovery behaviors are examined with different strain levels (up to 340% engineering strain). A multi-branched constitutive model that incorporates dilatational effects on the polymer relaxation time is established and applied to assist in discussions and understand the nonlinear viscoelastic behaviors of SMPs. It is shown that the volumetric dilatation results in an SMP network with lower viscosity, faster relaxation, and lower  $T_g$ . The influence of the dilatational effect on the thermomechanical behaviors is significant when the polymers are subject to large deformation or in a high viscosity state. The dilatation also increases the free recovery rate of SMP at a given recovery temperature. Even though the tested SMPs are far beyond their linear viscoelastic region when a large programming strain is applied, the free recovery behavior still follows the time-temperature superposition (TTSP) if the dilatational effect is considered during the transformation of time scales; however, if the programming strain is different, TTSP fails in predicting the recovery behavior of SMPs because the network has different entropy state and driving force during shape recovery. Since most soft active polymers are subject to large deformation in practice, this study provides a theoretical basis to better understand their nonlinear viscoelastic behaviors, and optimize their performance in engineering applications.

**Keywords** Mechanically-induced dilatation · Free volume · Shape memory polymer · Thermomechanical behaviors · Constitutive modeling

---

✉ K. Yu  
kai.2.yu@ucdenver.edu

<sup>1</sup> Department of Mechanical Engineering, University of Colorado Denver, Denver, CO 80217, USA

<sup>2</sup> State Key Laboratory of Science and Technology on Advanced Composites in Special Environments, Harbin Institute of Technology, Harbin 150080, P.R. China

## 1 Introduction

Shape memory polymers (SMPs) are smart materials that have the ability to recover their permanent shapes from one or sometimes multiple predetermined temporary shapes (Xie 2010; Luo and Mather 2010; Yu et al. 2012, 2015) when exposed to an environmental stimulus, such as temperature (Lendlein and Kelch 2002; Liu et al. 2007; Gall et al. 2005; Mather et al. 2009), magnetic field (Mohr et al. 2006; Schmidt 2006; Yakacki et al. 2009), light (Lendlein et al. 2005; Nagata and Yamamoto 2010; He et al. 2009) and solvents (Huang et al. 2005; Du and Zhang 2010; Boothby et al. 2017). In comparison with other shape memory materials like alloys and ceramics, SMPs exhibit unique and desirable properties including high programmable strain (over 400% reported in comparison with 8% in shape memory alloy Chen and Lagoudas 2008), light weight, and low cost among others; consequently these materials have attracted extensive research interests in recent years for applications in a wide array of fields such as actuation components in microsystems, biomedical devices, aerospace deployable, and morphing structures (Yakacki et al. 2007; Lendlein and Kelch 2005; Francis et al. 2007).

During the shape recovery of SMPs, polymer chains gradually relax towards their highest entropy configuration. Two major approaches are commonly used to model the thermomechanical behaviors of amorphous polymers, namely the free volume and configurational approaches. For the configurational approach, degrees of freedom of a glass is decomposed into a fast vibrational mode that equilibrates instantaneously and slow configurational modes that exist in a quasi-equilibrium state, characterized by an effective temperature. Such a modeling approach was extended by Xiao et al. to model the influence of the solvent (Xiao and Nguyen 2013) and deformation (Xiao and Nguyen 2015) on the viscoelastic behaviors of SMPs. For the free-volume-based modeling approach, the time scale is determined by the free volume and mobility of the polymer chains (Bower 2002; Ferry 1961). Numerous influential works have shown that increasing temperature will amplify the free volume and hence the shape recovery rate of SMPs. Such temperature dependency can be described using the time-temperature superposition principle (TTSP), which has served as a governing relationship for constitutive models developed by numerous researchers (Yu et al. 2014a,b; Nguyen et al. 2008; Westbrook et al. 2011; Diani et al. 2006; Srivastava et al. 2010). In addition, moisture will also increase the free volume and the mobility of polymer chains by weakening of secondary bonding forces (Huang et al. 2005). The temperature requirement for shape recovery is therefore reduced, and the SMPs actuate even at temperatures well below the required threshold of a dry specimen.

Previous work by Knauss and Emri (1981, 1987), Lu and Knauss (1999), Odowd and Knauss (1995) shows that in addition to temperature and moisture, mechanically-induced dilation (i.e. the macroscopic volume expansion of polymers during deformation) will also affect the time scale of polymers. For example, using the uniaxial stress relaxation tests on polyvinyl acetate, Knauss and Emri (1981) showed that specimens with higher strain levels relax faster at the same temperature. The higher relaxation rate essentially results from the increment in specimen volume after being stretched, which can be directly scaled with the increment of molecular free volume. Based on Doolittle's theory of polymer viscosity (Doolittle 1951, 1957), the influence of temperature, solvent, and dilatation on the polymer relaxation time was generalized into a single equation expressed as a linear combination of these parameters. Later, Liechti and coworkers (Chevellard et al. 2012; Popelar and Liechti 2003) extended this theory into the modeling of polymers with shear deformation. An effective strain was incorporated to include distortional effects on the viscosity of polymer. The model showed good predictions of creeping and stress-strain behavior for polyurea in pure shear tests.

This pioneering work demonstrates the significance of mechanically-induced dilatation on the time scale of polymers. However, little is known about its influence on the thermomechanical and shape memory behaviors of polymers intended for SMP applications. For example, how will the volumetric dilatation affect the transition temperature and shape recovery rate of SMPs, and how will it be coupled with geometrical nonlinearity and determine the performance of SMPs in a group? Such questions are important for many proposed SMP applications as the materials are usually subject to large deformation in practice. In this paper, we will study the influence of mechanically-induced dilatation on the behaviors of an acrylate-based amorphous SMP at large strain levels. Specifically, we will examine its temperature-dependent stress–strain, glass transition, and shape recovery behaviors for a range of uniaxial strain deformations. To assist in the discussion, a thermoviscoelastic model that incorporates mechanical dilatational effects on the relaxation time of SMPs will be established. The paper is arranged as follows: Sect. 2 contains the composition of the material selected for testing as well as the methodology use to test the thermomechanical and shape memory properties. Section 3 presents the theoretical model and the parameters identification method. Section 4 shows the comparison between model predictions and experimental results. With parametric studies based on the constitutive model, the influencing mechanism of the mechanically-induced dilatation on the thermomechanical and shape memory behaviors of SMPs is elaborated.

## 2 Materials and experiments

### 2.1 Material

The material used in this study is an acrylate-based amorphous SMP. Its liquid monomer *tert*-butyl acrylate (tBA), liquid cross-linker diethylene glycol (DEGDMA), and photo-initiator 2,2-dimethoxy-2-phenylacetophenone in powder form were all procured from Sigma Aldrich (St. Louis, MO, USA), and used without further modification or refinement. The synthesis procedure of the SMP followed Ortega et al. (2008) by mixing the tBA monomer, cross-linker and photo-initiator with a weight ratio of 100:4:1.04. The solution is then exposed in a UV irradiation for 15 min with a UV cross-linking oven (UVP LLC, Model CL-1000L, Upland, CA, USA).

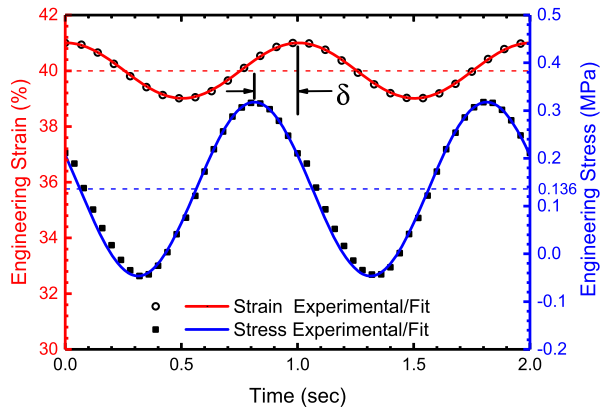
### 2.2 Thermal expansion tests

The coefficient of thermal expansion (CTE) of the acrylate SMP was measured using a dynamic mechanical analysis tester (TA Instruments, Model Q800, New Castle, DE, USA) machine. A rectangular specimen (22 mm × 4 mm × 1.6 mm) was mounted using the tensile testing apparatus. To measure the change in the specimen's length during thermal expansion or contraction, a constant and relatively small tensile force of 1 mN was applied and maintained during the entire experiment. The chamber temperature was first stabilized at 110 °C for 20 min and then the length of specimen was measured. From here the chamber temperature was decreased at 1 °C/min to a final temperature of 0 °C, while the length of the specimen was continuously monitored. The CTE of the SMP was evaluated in the rubbery region (i.e. above the transition temperature,  $T_g$ ) by calculating the curve slope in the linear region on the temperature-strain plot.

### 2.3 Glass transition behavior measurements

Previous work by Ortega et al. (2008) shows that with a dynamic strain of 0.1%, the synthesized acrylate SMP exhibits a  $T_g$  around 60 °C. Here, we are interested to examine how

**Fig. 1** Representative input strain (*upper sinusoidal curve*) and responsive stress (*lower sinusoidal curve*) during the dynamic mechanical tests on a 40% pre-strained specimen. Data shown represents two cycles at 64 °C with 1 Hz strain frequency and 1% dynamic strain amplitude. The experimental data is plotted in *symbols* and the analytical fittings are plotted in *continuous lines*



the strain level will affect  $T_g$ . Glass transition behavior of SMP specimens was investigated on the ElectroForce uniaxial tester (TA Instruments, Model 3230 Series II, New Castle, DE, USA) with a thermal control furnace (Sun Electronic Systems, Model ETI-1, Titusville, FL, USA).

Four rectangular specimens (22 mm  $\times$  4 mm  $\times$  1.7 mm) were first equilibrated at 65 °C for 15 min in the ElectroForce furnace, and then, respectively, stretched by 5%, 40%, 80%, and 120% engineering strain at 40 %/min. The specimens were cooled back to the room temperature (27 °C) to fix the applied deformation. The pre-strained specimen was then remounted in the grips to relieve the residual stresses, and subject to a sinusoidal uniaxial strain with amplitude of 1% and a frequency of 1 Hz. The dynamic strain oscillation was applied on the basis of the pre-strain. For example, the upper wave line in Fig. 1 shows the overall strain of the 40% strained specimen for 2 cycles during the tests, which was oscillating between 39% and 41%.

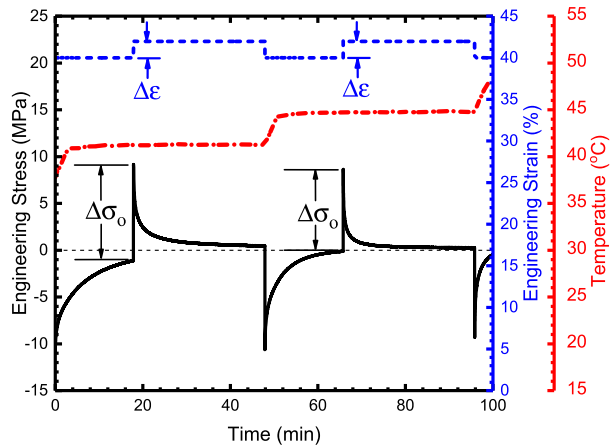
During the tests, the temperature was increased in discrete steps of 1.5 °C from room temperature ( $\sim$ 27 °C) to 110 °C. The heating rate between two temperature steps is 1.2 °C/min. A thermal equilibration of 20 min was applied at the beginning of each step, and followed by 30 cycles of strain waves. The stress response of the specimen was monitored during the controlled strain oscillations, and recorded at a rate of 60 data points per second.

The experimental data was fit using analytical sinusoidal functions with the same frequency of 1 Hz (solid lines in Fig. 1). The difference between the input strain waves and responsive stress waves determines the phase lag ( $\delta$ ) of polymer at different temperatures. The glass transition temperature ( $T_g$ ) of pre-strained specimens were determined to be the temperature corresponding to the peak value of  $\tan\delta$ , and the temperature-dependent storage modulus ( $E_s$ ) was calculated from the amplitudes of the stress and strain waves by  $E_s = \sigma_0/\varepsilon_0 \cos \delta$ .

## 2.4 Uniaxial tension tests

Uniaxial tension tests of the specimens were performed using the ElectroForce machine. The equilibrium stress–strain behavior of the SMP specimen (22 mm  $\times$  4 mm  $\times$  1.8 mm) was first examined. To eliminate the influence of the viscosity and isolate the purely elastic properties, testing temperature was set to be 80 °C, which is substantially beyond the  $T_g$ , while the strain was ramped at a quasi-static rate of 5%/min.

**Fig. 2** Representative subset of stress relaxation data for 40% pre-strained specimen conducted at 40.5 °C and 44 °C



Subsequently, the viscous stress–strain behavior of acrylate SMPs was measured with different temperatures and loading rates. A total of nine tensile tests were conducted. Specimens were heated to the prescribed temperature (55 °C, 60 °C and 70 °C, respectively) and stabilized for 20 min to ensure uniform thermal distribution. For each temperature, the specimens were extended to 340% engineering strain at rates of 17%/min, 85%/min, and 340%/min, respectively.

## 2.5 Stress relaxation tests

Stress relaxation testing was performed on the ElectroForce machine with stepwise increasing temperature and uniform strain amplitude deformations for a set of four SMP specimens. Each of these rectangular specimens (22 mm × 5 mm × 1.7 mm) was, respectively, stretched by 5%, 40%, 80% and, 120% engineering strain at 65 °C, and cooled to the room temperature to fix the applied deformation. The specimens were then remounted in the grips. For each specimen, a set of relaxation tests were conducted at increasing discrete temperatures range from 30 °C to 80 °C with 3.5 °C increments. At each temperature, the specimen was first stabilized for 30 min, and then subjected to a 2% step increase in strain. After stress relaxation for 30 min, the grips returned to their prior position with a 2% step decrease in strain.

A representative subset of experimental data for the 40% pre-strained specimen is shown in Fig. 2. It is noted that at the end of each relaxation step, the specimen tends to be compressed with the step decrease of strain, and a slight compressive stress might remain before the next relaxation step. Therefore, instead of using the absolute stress, the relative change in stress magnitude (as marked in Fig. 2) was used to calculate the relaxation modulus  $E(t)$  in relaxation step, i.e.  $E(t) = \Delta\sigma_i(t)/\Delta\varepsilon$ .

## 2.6 Shape memory tests

Shape memory characterization of acrylate SMPs was performed on the DMA machine. During the first step, rectangular specimens (8 mm × 4 mm × 0.9 mm) were held at a programming temperature ( $T_d$ ) of 70 °C for 10 min, and then, respectively, stretched by 5%, 40%, 80% and 120% engineering strain at 20%/min followed by an isothermal stabilization.

The total time for deformation and stabilization is 20 min for each case. After the temperature is reduced to the shape fixing temperature ( $T_L$ ) of 25 °C at 2 °C/min, the specimens underwent another isothermal stabilization for 30 min after which the load was released. This finishes the programming step. In the free recover step, the specimens were reheated to the target recovery temperature ( $T_r$ ) (60 °C and 70 °C, respectively) at 2 °C/min. Afterward the temperature is stabilized at  $T_r$  for 1 hour.

The shape recovery ratio ( $R_r$ ) is calculated according to the strain evolution in the recovery step as (Xie 2010; Lendlein and Langer 2002; Xie et al. 2011).

$$R_r(t) = 1 - \frac{\varepsilon(t)}{\varepsilon_p}, \quad (1)$$

where  $\varepsilon(t)$  represents the strain evolution during the free recovery step and  $\varepsilon_p$  is the programming strain maintained after unloading.

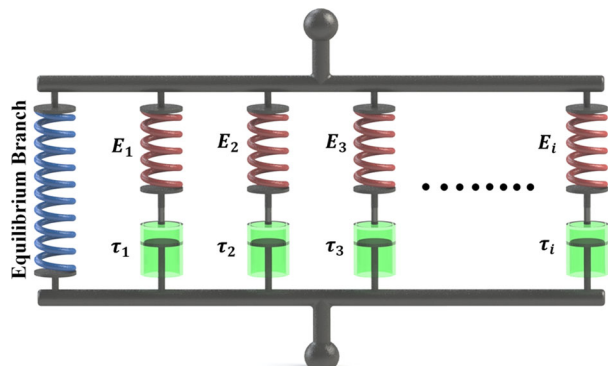
### 3 Theoretical modeling

A multi-branched constitutive model is applied to study the thermomechanical and shape recovery properties of acrylate SMPs at large strain amplitude. The model resembles a generalized Maxwell element that consists of one equilibrium branch and several thermoviscoelastic non-equilibrium branches (denoted by  $n$ ) arranged in parallel to represent the multiple relaxation processes (for example, Rouse modes) of the polymer. A schematic diagram of this model is presented in Fig. 3, where  $E_i$  and  $\tau_i$  are the elastic modulus and relaxation time in the  $i$ th non-equilibrium branch. The parameters and constitutive relations of equilibrium will be introduced later in this section. This paper presents the one dimensional (1D) nonlinear constitutive relation based on the multi-branched modeling frame. Methods for extending it into three dimensions can be found in work by Westbrook et al. (2011) and Diani et al. (2012).

Given the parallel arrangement of components comprising this model, the total stress is the sum of stress in each individual branch. The Cauchy stress of the multi-branched model  $\sigma$  is given by

$$\sigma = \sigma_{eq} + \sum_{i=1}^n \sigma_i, \quad (2)$$

**Fig. 3** Multi-branched thermoviscoelastic constitutive model for acrylate SMP



where  $\sigma_{eq}$  is the stress of equilibrium branch, and  $\sigma_i$  ( $i$  ranges from 1 to  $n$ ) is the stress in the  $i$ th non-equilibrium branch.

The stretch of each branch equals the stretch of the multi-branched model  $\lambda : \lambda = \lambda_{eq} = \lambda_i$ , where  $\lambda_{eq}$  and  $\lambda_i$  denote the stretch of equilibrium and the  $i$ th non-equilibrium branch, respectively. For the non-equilibrium branches, the stretch of the spring and dashpot elements are, respectively, denoted as  $\lambda_{i,m}$  and  $\lambda_{i,v}$ , where the subscript  $m$  denotes the elastic component and  $v$  the viscous.

### 3.1 Stress–strain relation in equilibrium branch

The stress–strain relation of the equilibrium branch is described by the Arruda–Boyce eight-chain model (Arruda and Boyce 1993) as shown in

$$\sigma_{eq} = \frac{nk_B T}{3} \frac{\sqrt{N}}{\lambda_{chain}} L^{-1} \left( \frac{\lambda_{chain}}{\sqrt{N}} \right) \left( \lambda^2 - \frac{1}{\lambda} \right), \tag{3}$$

where  $n$  is cross-linking density of acrylate SMP,  $k_B$  is Boltzmann’s constant,  $T$  is the absolute temperature,  $N$  is the number of Kuhn segments between two cross-link sites (Qi and Boyce 2004).  $\lambda_{chain}$  is the stretch ratio of polymer chains, which can be related to the macroscopic network deformation  $\lambda$  by  $\lambda_{chain} = \frac{1}{\sqrt{3}} \sqrt{\lambda^2 + \frac{1}{\lambda}}$ .

### 3.2 Stress–strain relation in non-equilibrium branches

Cauchy stress in the  $i$ th non-equilibrium branches ( $\sigma_i$ ) is represented by Eq. (4) for the spring component and Eq. (5) for the dashpot element of the Maxwell element:

$$\sigma_i = E_i \ln(\lambda_{i,m}), \tag{4}$$

$$\sigma_i = E_i \tau_i \frac{1}{\lambda_{i,v}} \frac{d\lambda_{i,v}}{dt}. \tag{5}$$

In the preceding equations,  $E_i$  and  $\tau_i$  refer to the  $i$ th branch elastic modulus and relaxation time, respectively.

### 3.3 Relaxation time and time-temperature shift factor

For the non-equilibrium behaviors in the viscoelastic branches, it is assumed that all branches follow the same viscous flow rules but with different relaxation times. According to the well-established “thermo-rheological simplicity” principle (Rubinstein and Colby 2003) under a non-isothermal condition, the relaxation times (or viscosity) of each non-equilibrium branch vary as the temperature changes:

$$\tau_i(T) = \tau_{i0} \alpha(T), \tag{6}$$

where  $\alpha(T)$  is the temperature-dependent shift factor,  $\tau_{i0}$  is the  $i$ th branch relaxation time at the reference temperature when  $\alpha(T) = 1$ .

Following Knauss and Emri (1981, 1987), Lu and Knauss (1999), Odowd and Knauss (1995), we assume the mechanically-induced dilatation affects the thermomechanical properties of polymer by changing the temperature-dependent shift factor  $\alpha(T)$ . Doolittle ex-

pressed the shift factor in terms of the free volume of polymer chains (Doolittle and Doolittle 1957):

$$\log_{10}[\alpha(T)] = -\frac{B}{2.303} \left( \frac{1}{f} - \frac{1}{f_0} \right), \quad (7)$$

$$f = \frac{v_f}{v_f + v_0} \approx \frac{v_f}{v_0}, \quad \text{since } v_f \ll v_0, \quad (8)$$

where  $B$  is a material specific constant,  $f$  is the fractional free volume  $f_0$  is the fractional free volume at a given reference temperature.  $v_0$  is the solid volume and  $v_f$  is the free volume of polymer chains.

According to Knauss and Emri (1981, 1987), Lu and Knauss (1999), Odowd and Knauss (1995), the fractional free volume of a dry polymer depends on the linear combination of temperature  $T$  and mechanically-induced dilation  $\theta$ :

$$f = f_0 + \alpha_v(T - T_M) + \delta\theta, \quad (9)$$

where  $T_M$  is a reference temperature associated with  $f_0$ ,  $\alpha_v$  is the coefficient of thermal expansion,  $\delta$  represents a fitting factor, which will be determined in the following section by comparing model predictions on uniaxial stress–strain behaviors with experimental data.

Substituting Eq. (9) into Eq. (7) we will have

$$\log_{10}[\alpha(T, \theta)] = -\frac{B}{2.303 f_0} \frac{\alpha_v(T - T_M) + \delta\theta}{f_0 + \alpha_v(T - T_M) + \delta\theta}. \quad (10)$$

If the mechanical dilation is considered to be negligible (with  $\delta = 0$ ), it can be seen that Eq. (10) simply reduces to the classic Williams–Landel–Ferry (WLF) equation (Williams et al. 1955):

$$\log_{10} \alpha(T) = -\frac{C_1(T - T_M)}{C_2 + (T - T_M)}. \quad (11)$$

Comparing Eqs. (10) and (11) we have  $C_1 = -\frac{B}{2.303 f_0}$ , and  $C_2 = \frac{f_0}{\alpha_v}$ . So Eq. (10) is rewritten as:

$$\log_{10}[\alpha(T, \theta)] = -\frac{C_1(T - T_M) + \frac{\delta C_1 \theta}{\alpha_v}}{C_2 + (T - T_M) + \frac{\delta}{\alpha_v} \theta}. \quad (12)$$

The mechanically-induced dilation  $\theta$  can be expressed using the three principal stretch parameters  $\lambda_1$ ,  $\lambda_2$  and  $\lambda_3$ . With the axis of uniaxial tension aligned with the  $\lambda_1$  stretch direction, these three terms can be related by the Poisson ratio  $\nu$  where  $\lambda_1 = \lambda$  and  $\lambda_2 = \lambda_3 = \lambda^{-\nu}$ . The volumetric mechanical dilation term can be expressed as

$$\theta = \frac{\Delta V}{V_0} = \lambda_1 \lambda_2 \lambda_3 - 1 = \lambda^{1-2\nu} - 1. \quad (13)$$

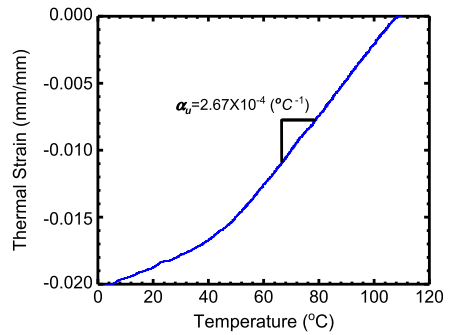
Here, we express the Poisson ratio by using the elastic moduli (Tschoegl et al. 2002; Lakes and Wineman 2006)

$$\nu(t, T) = \frac{1}{2} - \frac{1}{6} \frac{E(t, T)}{K}, \quad (14)$$

where  $E(t, T)$  is the relaxation modulus of the multi-branched model,  $K$  is the bulk modulus of the material, which is chosen to be independent of the temperature (Westbrook et al.



**Fig. 4** Thermal-expansion curve generated through constant cooling (1 °C/min) from a reference point at 110 °C to 0 °C



2011) and is typically orders of magnitude larger than the modulus. In the previous viscoelastic models for SMPs, a large value of bulk modulus was assumed to ensure the material incompressibility. However, if the free-volume-based viscoelastic model is adopted to study the thermomechanical behaviors of polymers at large deformation, one might consider the variation of Poisson’s ratio around glass transition region. For example, Greaves et al. (2011) showed that, as the increment of the temperature across  $T_g$ , the polymers’ Poisson’s ratio gradually increases from the initial value of  $\sim 0.33$  in glassy state to the incompressible value of 0.5 in rubbery state. In this paper, we set the bulk modulus of polymer to be 1.3 GPa, which is  $\sim 10000$  times of the equilibrium shear modulus (0.13 MPa), and  $\sim 1.1$  times of the instantaneous modulus of the multi-branched model. Since bulk modulus is related to the Poisson ratio by Eq. (14), a change in its value will notably affect the viscoelastic predictions.

The shift factor in Eq. (12) is applicable to temperatures in the region governed by the WLF equation (above a shift temperature  $T_s$ ). As will be shown in the following section, when the temperature is below  $T_s$ , the shift factor is independent of the strain amplitude other than temperature. In this region the shift factor for the reference relaxation times can be expressed through the Arrhenius equation (Arrhenius 1889)

$$\ln[\alpha(T)] = -\frac{AF_c}{k_b} \left( \frac{1}{T} - \frac{1}{T_g} \right), \tag{15}$$

where  $A$  and  $F_c$  material specific constants.  $T_s$  is taken to be the crossing point of two curves representing Eqs. (16a)–(16c) and (12) on a  $\alpha$  vs.  $T$  plot.

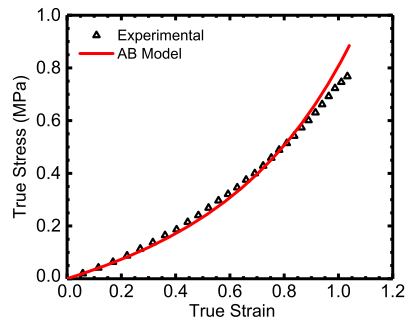
### 3.4 Material parameters identification

This section will introduce the identification methods for the four groups of material parameters in the multi-branched model: the thermal-expansion coefficient, parameters in the equilibrium branch, the TTSP parameters, elastic moduli and relaxation times of non-equilibrium branches.

#### 3.4.1 Thermal expansion coefficient

Thermal-expansion properties of acrylate SMPs were evaluated from the strain evolution response to a linearly decreasing temperature ramp (Fig. 4). As shown in the figure, the linear regression at temperatures above  $T_g$  is taken to be the CTE in the rubbery region. Here the uniaxial rubbery linear CET is  $\alpha_u = 2.67 \times 10^{-4} \text{ }^\circ\text{C}^{-1}$ , and the volumetric CTE of acrylate SMP is determined to be  $\alpha_v = 3\alpha_u = 8.01 \times 10^{-4} \text{ }^\circ\text{C}^{-1}$

**Fig. 5** True stress–strain curve of acrylate SMP at 80 °C with low strain rate ( $\dot{\epsilon} = 5\%/min$ ). Note: *solid line* is the experimental data and *dashed line* is the prediction from Arruda–Boyce model



### 3.4.2 Parameters in the equilibrium branch

The equilibrium branch parameters are used to characterize the hyperelastic behavior of the material at temperatures above  $T_g$ . The cross-linking density  $n$ , and the number of Kuhn segments  $N$  of the Arruda–Boyce (AB) eight-chain model can be determined by using a single uniaxial tension test. The true stress–strain curve of the acrylate SMP at 80 °C is shown by the solid line in Fig. 5. By fitting to the experimental data, the parameters in the equilibrium branch are determined to be  $n = 6.2 \times 10^{25}$  and  $N = 23.4$ .

### 3.4.3 TTSP parameters

The TTSP parameters  $C_1$  and  $C_2$  (in Eq. (12)) and  $AF_c k_b^{-1}$  (in Eqs. (16a)–(16c)) are determined using the results in temperature-dependent stress relaxation tests on SMP specimen with 5% pre-strain. It is noted that the 5% pre-strain was used to keep the experimental procedure to be consistent for all SMP specimens. However, since the pre-strain is small, its influence on the volumetric dilatation and relaxation time scale is expected to be negligible. The relaxation modulus of acrylate SMP at 17 temperatures is presented on a double logarithmic plot in Fig. 6. It is seen that the stress relaxation modulus is strongly dependent on the testing temperature.

The collected data was then shifted into a master curve to represent the polymer stress relaxation behavior over an extended time regime (Fig. 6(b)). For the acrylate SMP, DMA measurement reveals a  $T_g$  at 66.7 °C with small strain level (5%). For a typical polymer, the reference temperature  $T_M$  (in Eq. (13)a) should be about 5–15 °C below  $T_g$ . Therefore, in the applied multi-branch model,  $T_g$  is set to be 66.7 °C and  $T_M$  is 54 °C. The corresponding  $T_s$  is 44 °C. Selecting  $T_s$  as the reference temperature, each curve in Fig. 6(a) was shifted horizontally to superimpose with the next. This produced a master curve that represents the actual relaxation behavior of the acrylate SMPs within a long time scale ( $\sim 31$  years) at 44 °C. It is noted that the relaxation spectrum of an amorphous network can also be obtained from the master curve of frequency-dependent storage modulus, as previously showed by Nguyen et al. (2010). These two approaches should be equivalent when the deformation of amorphous networks is in the linear region.

The shifting factors  $\alpha(T)$  are plotted as a function of temperature in Fig. 6(c). As described in Eqs. (12) and (15), the shifting factors follow the WLF and Arrhenius equations when the temperature is, respectively, above and below  $T_s$ . By fitting the experimental data with the theoretical predictions, the parameters in these two equations are determined as:  $C_1 = 11.00$ ,  $C_2 = 33.6$  °C, and  $AF_c k^{-1} = -50500$ .

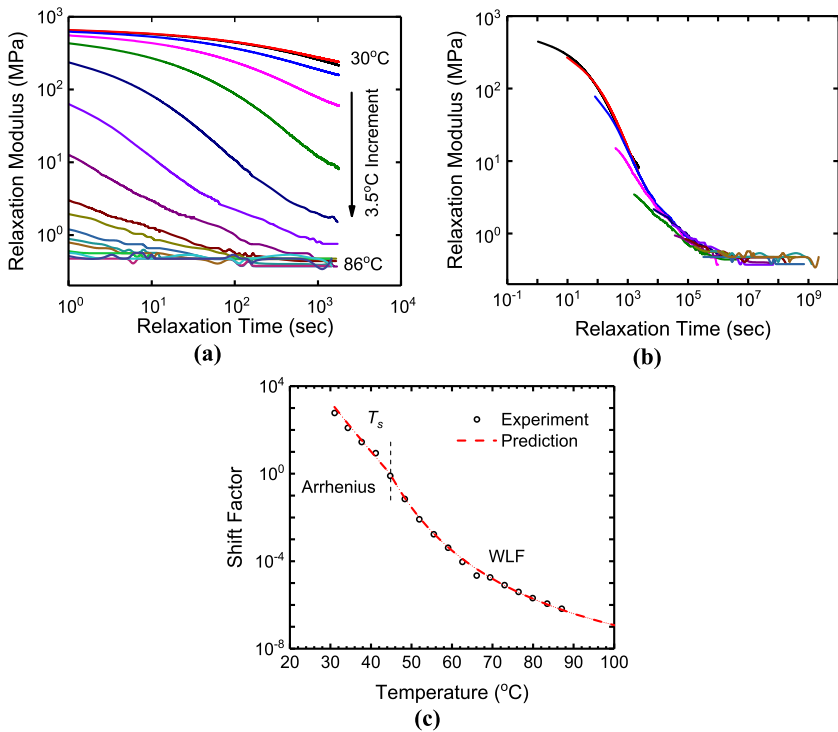


**Fig. 6** (a) Stress relaxation tests at 17 different temperatures (30 °C–86 °C with 3.5 °C increment); (b) the stress relaxation master curve at 44 °C; (c) shifting factors at different temperatures: above 44 °C, shifting factors follow the WLF equation; below 44 °C, shifting factors follow the Arrhenius-type behavior

### 3.4.4 Elastic moduli and relaxation times of non-equilibrium branches

By using nonlinear regression (NLREG) method (Diani et al. 2012; Sherrod 2000), the modulus and relaxation time in each branch were estimated by fitting the model prediction with the experimental DMA results. The solid lines in Fig. 7 plot the measured storage modulus and  $\tan \delta(T)$  as a function of temperature, where the strain amplitude is 5%, so the dilatational effect is negligible. For the 1D multi-branched model without consideration of the volumetric dilatation, the temperature-dependent storage modulus  $E_s(T)$ , loss modulus  $E_l(T)$  and  $\tan \delta(T)$  are, respectively, expressed as

$$E_s(T) = E_{eq}(\lambda) + \sum_{i=1}^n \frac{E_i [\tau_i(T)]^2 \omega^2}{1 + [\tau_i(T)]^2 \omega^2}, \tag{16a}$$

$$E_l(T) = \sum_{i=1}^n \frac{E_i \tau_i(T) \omega}{1 + [\tau_i(T)]^2 \omega^2}, \tag{16b}$$

$$\tan[\delta(T)] = \frac{E_l(T)}{E_s(T)}, \tag{16c}$$

where  $\omega$  is the testing frequency,  $\tau_i$  is the relaxation time in each non-equilibrium branch, and  $E_i$  is the corresponding elastic modulus. Due to the nonlinear stress–strain relation of

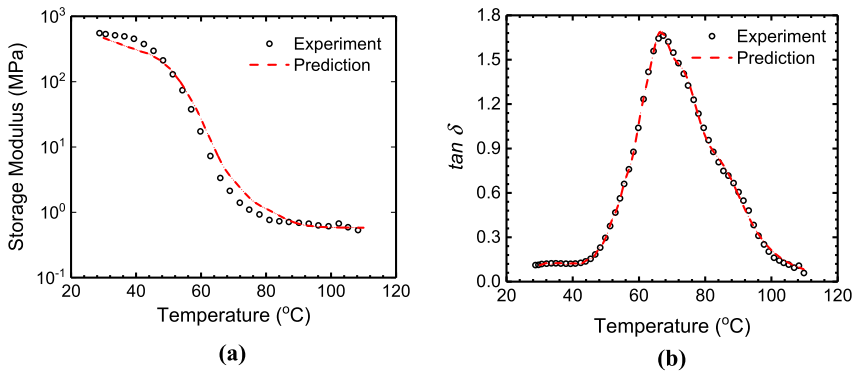


**Fig. 7** Comparisons between the experimental results and model prediction on (a) storage modulus and (b)  $\tan \delta$

**Table 1** Elastic moduli and relaxation times in each respective non-equilibrium branch ( $n = 12$ )

$E_i$ (MPa)	$2.00 \times 10^2, 7.68 \times 10^1, 6.47 \times 10^1, 5.16 \times 10^1, 5.12 \times 10^1, 5.96 \times 10^1, 6.94 \times 10^1,$ $5.83 \times 10^1, 1.05 \times 10^1, 3.43 \times 10^1, 2.12 \times 10^0, 5.96 \times 10^0$
$\tau_{i0}$ (s)	$4.47 \times 10^{-5}, 1.00 \times 10^{-3}, 9.08 \times 10^{-3}, 8.70 \times 10^{-2}, 8.91 \times 10^{-1}, 8.44 \times 10^0, 6.33 \times 10^1,$ $3.72 \times 10^2, 1.00 \times 10^4, 2.11 \times 10^3, 8.42 \times 10^4, 8.32 \times 10^5$

rubbery polymers at large deformation, the equilibrium modulus in Eq. (16a) is taken to be a function of uniaxial stretch, i.e.  $E_{eq}(\lambda)$ , which is calculated by the first order derivative of equilibrium stress (Eq. (3)) over the true strain  $\ln(\lambda)$ .

During the nonlinear regression analysis, non-equilibrium branches are gradually added into the model to improve the prediction, and the branch number is finally determined when the NLREG estimations (shown as dash lines in Fig. 7) could capture the experimental storage and  $\tan \delta$  curves within the entire testing temperature range (30  $^{\circ}\text{C}$  to 110  $^{\circ}\text{C}$ ).

For the acrylate used in the development of this model, a total of 12 branches were required to fit the suitably fit the experimental curves (Fig. 7). The relaxation times and elastic moduli are listed sequentially for each respective branch in Table 1.

## 4 Results and discussion

### 4.1 Uniaxial tension behavior

The comparisons between model predictions and experimental results of stress–strain curves in uniaxial tension tests are shown in Figs. 8(a), 8(c), and 8(e), where at each temperature (55  $^{\circ}\text{C}$ , 60  $^{\circ}\text{C}$  and 70  $^{\circ}\text{C}$ ), the material was, respectively, stretched to 340% engineering strain (1.481 true strain) with three strain rates (17%/min, 85%/min and 340%/min in engineering strain rate, 0.157/min, 0.615/min, 1.481/min in true strain). It is seen that the when the fitting parameter  $\delta$  in Eq. (9) is set to be 0.089, the model predictions (dashed lines) on the uniaxial stress–strain curves agree well with the experimental data (solid lines). As shown by the stress–strain curves, the acrylate SMP displays a highly viscous behavior at 55  $^{\circ}\text{C}$  and 60  $^{\circ}\text{C}$ , with uniaxial stress dramatically increasing with loading rate. At 70  $^{\circ}\text{C}$ , the

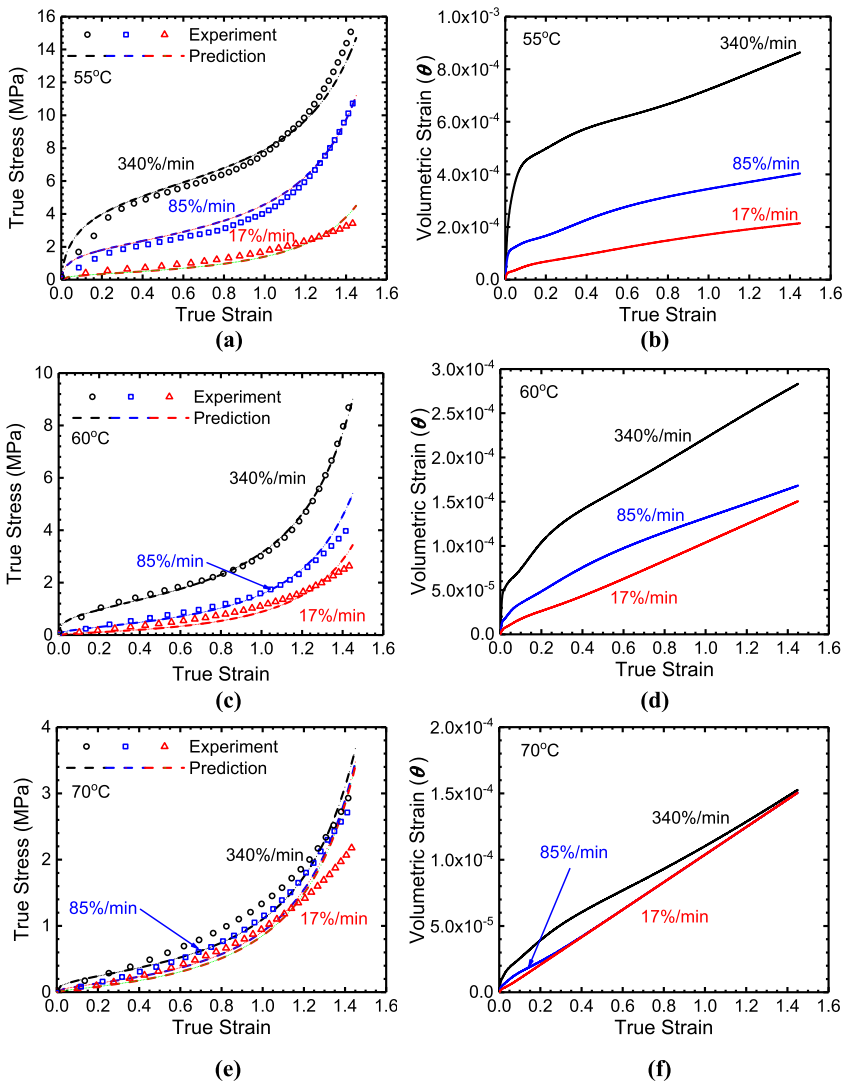


**Fig. 8** (a), (c) and (e) compare the model predictions and experimental results of uniaxial tensile test at varying temperatures and strain rates. (b), (d) and (f) show the corresponding evolution of volumetric dilation ( $\theta$ ) during the tension tests

material exhibits a typical hyperelastic behavior of rubbery materials with slight influence from loading rate.

Predictions of the volumetric dilation ( $\theta$ ) evolution during the corresponding uniaxial tension tests in Figs. 8(a), 8(c), and 8(e) are provided in the adjacent graphs (Figs. 8(b), 8(d), and 8(f)). These curves demonstrate that the dilation is closely related to the polymer’s macroscopic deformation. As shown in Eqs. (13) and (14),  $\theta$  increases nonlinearly with the network stretch ratio  $\lambda$  with an exponential power of  $1-2\nu$ . Even though rubbery polymers are commonly considered to be incompressible with  $\nu = 0.5$ , such condition can never be reached as it requires an infinitely large bulk modulus. A Poisson ratio below 0.5 leads to

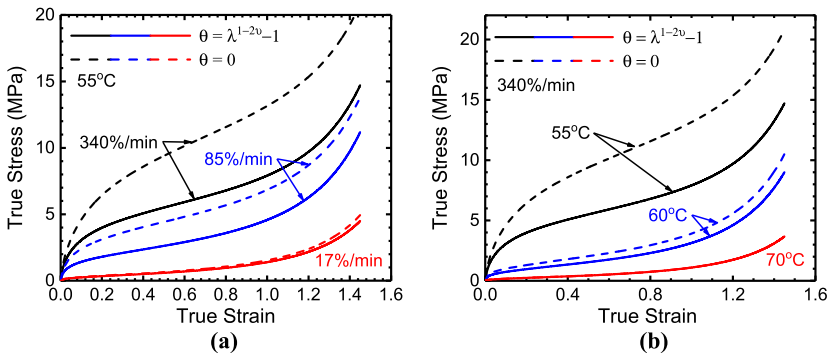


**Fig. 9** Comparison of theoretical predictions for uniaxial testing results with (solid lines) and without (dashed lines) mechanically-induced dilation as a model parameter. (a) Constant temperature (55 °C) with varying strain rates and (b) constant strain rate (340%/min) with varying temperatures

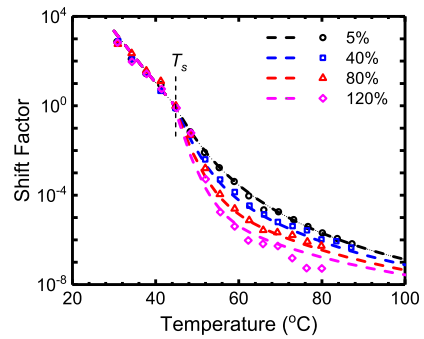
volumetric dilation of SMP network, which tends to be notable at large deformation. In addition, the Poisson ratio is even smaller when viscous effect was considered in Eq. (14), where the mechanical dilation depends on the polymer's relaxation modulus. During rapid straining or at low temperatures, the high viscosity of the SMP results in a higher relaxation modulus and increased volumetric dilation. The increment in polymer macroscopic volume is translated into free volume of polymer chains, which increases their mobility and reduces the viscosity in turn. While at 70 °C, there is little influence of strain rate in this low viscosity state. The mechanical dilation depends almost exclusively on macroscopic straining. This results in the dilation functions collapsing towards a single curve with little dependency on the strain rate.

To elucidate the significance of mechanical dilation on the prediction of SMP behavior at large deformation, the theoretical model was run under the same conditions for uniaxial tension tests, however, the mechanical dilation parameter in Eq. (12) was set to be zero ( $\theta = 0$ ). The results of each run were then compared with the predictions in Fig. 8. The stress–strain curves at 55 °C with three strain rates, and the stress–strain curves with the same loading rate of 340%/min at three different temperatures are, respectively, shown in Figs. 9(a) and 9(b). Because mechanical dilation increases the free volume of polymer chains, failure to account for this factor results in a predicted polymer behavior with higher viscosity. As shown in Fig. 9, without consideration on the dilatational effect, i.e.  $\theta = 0$ , the model considerably overestimates the stress response of the polymer at low temperature or high loading rate. While at high temperature or with low loading rate, the difference between these two model predictions tends to be negligible. These results demonstrate that mechanical dilation is required for accurate constitutive modeling on the thermomechanical behavior of SMPs, especially when the polymers are in a high viscoelastic state.

## 4.2 Strain amplitude dependent TTSP

Stress relaxation tests were performed on SMP specimens with different pre-strain levels (5%, 40%, 80% and, 120% engineering strain). Then for each specimen, their temperature-dependent stress relaxation curves were shifted to construct a master relaxation curve with the same reference temperature  $T_s = 44$  °C (see Sect. 3.3 for a detailed procedure). The corresponding shift factors of four SMP samples are plotted in Fig. 10, where the geometric dots represent experimental data, and the solid/dash lines show the model predictions.

**Fig. 10** TTSP shift factors of four SMP samples with 5%, 40%, 80% and 120% pre-strain. *Geometric dots* represent experimental data, while *solid/dashed lines* show model predictions



From the figure, it is apparent that in the region below the shift temperature ( $T_s$ ) the pre-strain has little influence on the relaxation behavior of SMPs. The shift factor curves essentially overlap into a single line which can be captured using the Arrhenius equation (Eq. (15)). The reason is that at low temperature (below  $T_s$ ), the free volume of polymer chains is significantly reduced, so the influence of mechanical dilation on the thermomechanical behavior of SMPs tends to be negligible.

At higher temperatures (above  $T_s$ ), conversely, samples with increased pre-strain exhibit more rapid decrease in shift factors compared to those of lower strained samples. This can be seen as a consequence of amplified free volume resulting from increased mechanical dilation. The increased chain mobility leads to a reduced viscosity of SMPs, which enables the network to release internal stress more quickly. When constructing the master relaxation curve, each relaxation curve must be shifted further to the right; the result of which is the lower shift factors at equivalent temperatures. The developed constitutive model shows a close prediction on the strain amplitude dependent TTSP shift factors as seen from the solid/dashed lines in Fig. 10.

It is noted that the adopted free-volume modeling approach for amorphous SMPs assumes that the interactions among macromolecular chains has no influence on the time scale of polymers during viscoelastic deformation. However, caution should be taken when using the model to study the viscoelastic deformations in compression condition. In the supplementary material, we tested the relaxation behaviors of acrylate SMPs in compression condition. Cylindrical samples (diameter = 10 mm, height = 10 mm) were fabricated and subject to uniaxial compression on a MTS machine at 60 and 70 °C, respectively. The compressive strain was set to be 5%, 40%, and 60%, respectively. The experimental results show that at the same temperature, the time scale for stress relaxation has no significant difference among different strain levels. The reason is that in a compression state, the repulsive forces among polymer chains may start to play a role, which prevents the free volume of chains from continuously reducing, so the network mobility has no significant change at high strain levels. Meanwhile, in the tension state, the influence of chain interactions could be a minor effect, as the polymer chains tend to separate from each other.

### 4.3 Strain amplitude dependent glass transition behavior

Mechanically-induced dilation would also affect the dynamic mechanical behavior of polymers by changing the free volume of polymer chains. The glass transition behaviors of four SMP specimens with different levels of pre-strain are shown in Fig. 11. From Fig. 11(a), it appears that the mechanical dilatation has little influence on the storage modulus as all

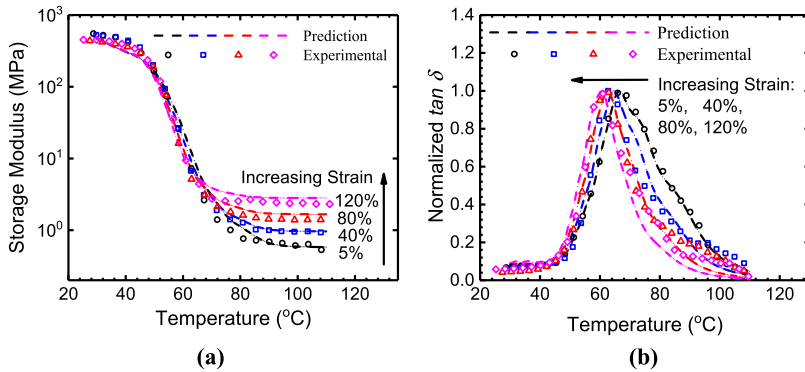


**Fig. 11** Experimental results (solid lines) and theoretical predictions (dashed lines) of storage modulus (a) and  $\tan \delta$  (b) for four pre-strained samples (5%, 40%, 80% and 120%)

the four curves are overlapped before reaching the rubbery plateaus. This is essentially resulted from the combined influences from both dilatation and nonlinear rubbery modulus of SMPs at large deformation: first, volumetric dilatation increases the free volume of polymer chains, which has the same effect of increasing temperature in lowering the storage modulus; second, due to the extension and alignment of polymer chains at larger deformation, SMPs with higher pre-strain exhibits higher equilibrium modulus, which in turn increases the storage modulus (see Eq. (16a)). For example, as shown in Fig. 11(a), the rubber modulus of 120% pre-strained sample is  $\sim 1.8$  MPa at 100 °C, which is  $\sim 300\%$  higher than that of 5% pre-strained sample ( $\sim 0.45$  MPa). Since the increment in equilibrium modulus is almost in the same range as the storage modulus of SMPs when the mechanical dilatation is effective ( $\sim 55$  °C as revealed from Fig. 10), these two influencing factors tend to be canceled out and the storage moduli of the four samples evolve consistently.

However, peaks of the  $\tan \delta$  curves in Fig. 11(b) are seen to be shifted to a lower temperature when higher pre-strain is applied, which means the mechanical dilatation effectively lowers the  $T_g$  of SMP samples. On increasing the pre-strain from 5% to 120%, the  $T_g$  is reduced from 66.7 °C to 61.0 °C. For both storage modulus and  $\tan \delta$  curves shown in Fig. 11, the model prediction fit well with the experimental data.

#### 4.4 Shape memory behavior with different programming strain

The shape memory behavior of acrylate SMPs was tested with different amplitudes of programming strain. During the shape memory tests, the SMP samples were strained to 5%, 40%, 80% and 120% at the same programming temperature of 70 °C. After unloading at 25 °C, all the SMP specimens were able to completely fix the programming deformation. In the free recovery step, the samples were subjected to free standing heating at 60 °C and 70 °C, respectively.

The solid lines in Fig. 12 show the shape recovery ratio of these specimens in the respective tests, and the corresponding model predictions are given as the dashed lines. The close comparison of the model predictions to the experimental recovery data demonstrates the effectiveness of the theoretical model in predicting the strain amplitude dependent shape recovery behavior. It is also seen from the figure that a higher programming strain results in faster shape recovery at a given temperature. This results mainly for two reasons: first, a higher programming strain leads to a higher level of mechanical dilatation stored in the



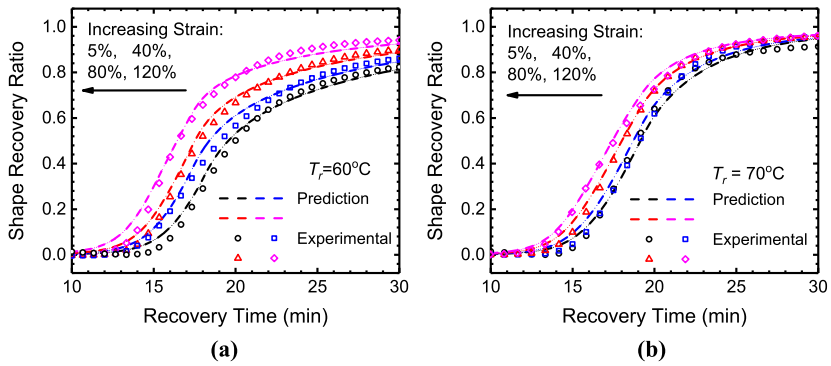


**Fig. 12** Shape recovery behavior of SMP samples at recovery temperatures of (a) 60 °C and (b) 70 °C. The programming strain was set to be 5%, 40%, 80% and 120%. Theoretical model predictions are given as dashed lines

SMP, which contributes to increase the mobility of polymers chains when the network is reactivated in the recovery step. The SMP therefore exhibits a higher shape recovery rate at a given temperature. Second, as shown in the previous work (Yu and Qi 2014), the stress in the equilibrium branch of the multi-branched model is providing the driving force for the shape recovery of SMPs. The equilibrium stress will increase nonlinearly with the programming strain (following Eq. (3)), which is stored in the network at low temperature and subsequently increases the shape recovery rate of unconstrained SMPs. It is therefore concluded that the level of programming strain increases the shape recovery rate of SMPs by promoting the mobility of polymer chains and increasing the driving force for network shape recovery.

In previous work (Yu et al. 2014a), it was shown that by using the same programming conditions, the free recovery behavior of amorphous SMPs followed TTSP, where the reduced time is serving as a unified parameter to predict the temperature-dependent shape recovery curves. The governing equations are presented as:

$$R_r = R_r(t_r), \tag{17a}$$

$$t_r = \int \frac{dt}{\alpha}. \tag{17b}$$

Equations (17a) and (17b) demonstrate that the recovery ratio  $R_r$  only depends on the reduced time  $t_r$ , which is the physical time divided by the TTSP shift factors  $\alpha(T)$ . This conclusion was reached with the assumption of small deformation and linear viscoelastic behavior of polymers. Without considering the dilatational effect,  $\alpha(T)$ , respectively, follows the WLF (Eq. (11)) and Arrhenius (Eq. (15)) equations above and below  $T_g$ .

Here, we demonstrate that this principle is still applicable when the SMPs are far beyond their linear viscoelastic region within the shape memory cycle. First, the free recovery behaviors of acrylate SMPs with different programming strains (5% and 120%) and different recovery temperatures (55 °C, 60 °C, 65 °C and 70 °C) are predicted using the multi-branched constitutive model. The other programming and recovery conditions are identical, where SMP samples were strained at the same programming temperature ( $T_d = 65$  °C) and then stabilized for a total of 20 min; after cooling to the shape fixing temperature ( $T_L = 25$  °C) at 2 °C/min and stabilizing for 30 min, the external load was removed and the

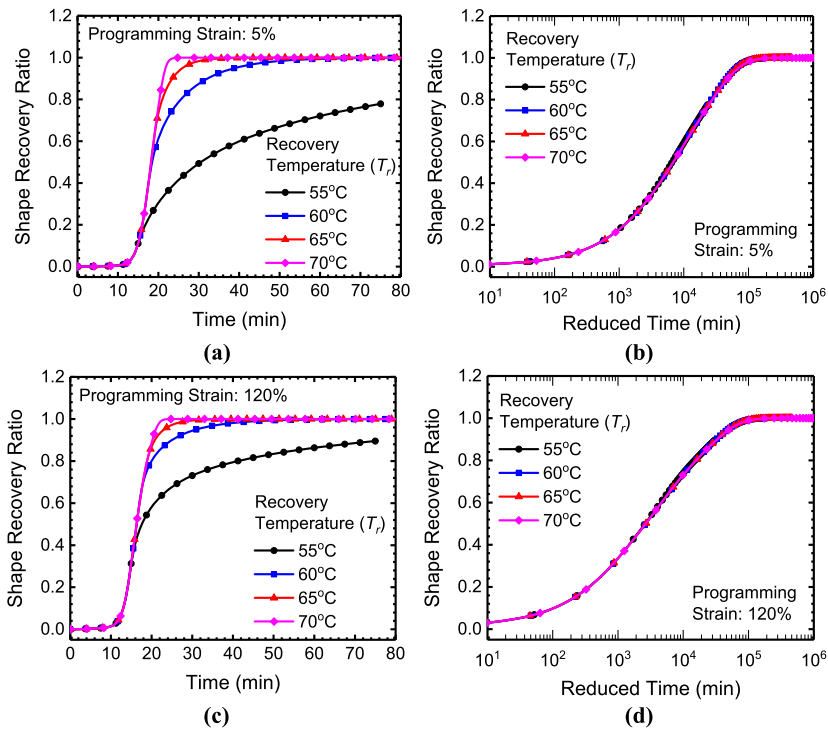


**Fig. 13** TTSP for the free recovery behavior of acrylate SMPs at large strain deformations with the consideration of the dilatational effect. (a) Shape recovery ratio curves at 5% strain deformation for four recovery temperatures, (c) shape recovery ratio curves at 120% strain deformation for four recovery temperatures, (b and d) recovery ratio master curves for 5% and 120% programming strains, respectively

SMP was subjected to unconstrained shape recovery. The temperature was ramped to the target at 2 °C/min. The predicted shape recovery curves are plotted in Figs. 13(a) and 13(c).

Subsequently, the physical time scale in Figs. 13(a) and 13(c) are transformed into the reduced time scale following Eq. (17b). With the consideration of nonlinear large deformation and mechanical dilatation effect, Eq. (12) is adopted to express the TTSP shift factor  $\alpha(T, \theta)$ . The free recovery curves after time scale transformation are shown in Figs. 13(b) and 13(d). It is seen that, for each case of programming strain, the four recovery curves at different temperatures rejoin to form a free recovery master curve, which indicates that when using the same programming strain, the recovery behavior of SMPs follows the TTSP even at large deformation with nonlinear viscoelastic behavior.

The question remains, if the recovery behavior of SMPs still follows TTSP when they are subject to the same recovery temperature but different amplitudes of programming strain. In Fig. 14(a), the recovery curves are predicted using the multi-branched model with the same programming and recovery temperature ( $T_d = 65$  °C,  $T_r = 60$  °C), but four different the programming strains. The recovery curves after transforming the time scale using Eq. (17b) and Eq. (12) are shown in Fig. 14(b). It is evident that the curves are not converging. This is because after unloading at a low temperature the SMP network has different states of entropy and internal energy, which provides different levels of driving force for shape recovery (Yu and Qi 2014). Since this difference only depends on the magnitude of applied programming strain, a master curve cannot be obtained after time scale transformation. It is

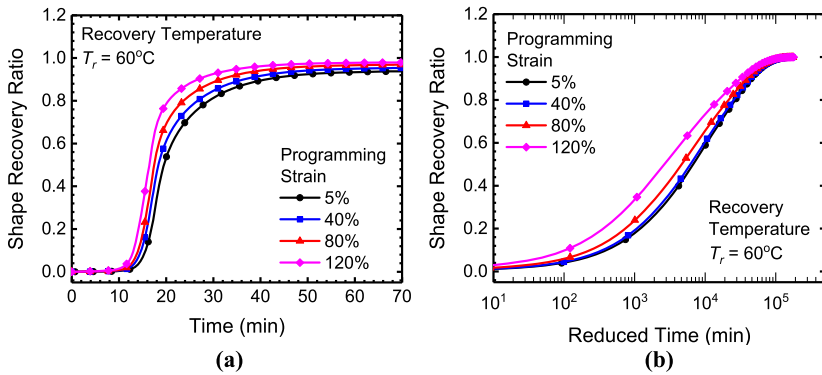


**Fig. 14** (a) Simulation prediction of recovery ratios for four specimens subjected to pre-strains of 5%, 40%, 80% and 120% exposed to the same recovery conditions in physical time. (b) The same curves as (a) shifted into reduced time using dilation parameterized shift factor. Convergence of the curves cannot be achieved due to differing programming histories

therefore concluded that TTSP fails in predicting the recovery behavior of SMPs when they are subject to different programming strains.

## 5 Conclusion

In the paper, we investigated the influence of macroscopic volume expansion of polymers during deformation, i.e. the mechanically-induced dilatation, on the thermomechanical and shape memory behaviors of amorphous shape memory polymers (SMPs). Experimental results revealed that the volumetric dilatation plays the same role as increasing temperature in reducing the polymer viscosity. With higher strain levels, SMPs exhibit a stress–strain behavior with lower viscosity, a faster stress relaxation, a lower glass transition temperature, and a higher rate of shape recovery. The underlying mechanism results from a Poisson ratio smaller than 0.5, this causes the polymer to expand in volume under uniaxial tension. The macroscopic volume expansion is scaled with the free volume-increment of macromolecular chains, which enhances their mobility at equivalent temperatures. The dilatational effect is more observable when the polymer is in the viscoelastic region with a smaller Poisson ratio and larger volume expansion. A multiple branched constitutive model with the consideration of the dilatational effect is established, which provides a close prediction for the behaviors of SMPs. Parametric studies show that the free recovery of SMP follows the time-temperature superposition principle even at large deformation with nonlinear viscoelastic behavior. However, if the SMPs are programmed with different strain levels, TTSP fails to predict the recovery ratio due to the different entropy and internal energy states prior to shape recovery.

## References

- Arrhenius, S.: Über die Reaktionsgeschwindigkeit bei der Inversion von Rohrzucker durch Säuren. *Z. Phys. Chem.* **4**, 226–248 (1889)
- Arruda, E.M., Boyce, M.C.: A three-dimensional constitutive model for the large stretch behavior of rubber elastic materials. *J. Mech. Phys. Solids* **41**, 389–412 (1993)

- Boothby, J.M., Kim, H., Ware, T.H.: Shape changes in chemoresponsive liquid crystal elastomers. *Sens. Actuators B, Chem.* **240**, 511–518 (2017)
- Bower, D.I.: *An Introduction to Polymer Physics*. Cambridge University Press, New York (2002), xx, 444 pp.
- Chen, Y.C., Lagoudas, D.C.: A constitutive theory for shape memory polymers. Part I—Large deformations. *J. Mech. Phys. Solids* **56**, 1752–1765 (2008)
- Chevellard, G., Ravi-Chandar, K., Liechti, K.M.: Modeling the nonlinear viscoelastic behavior of polyurea using a distortion modified free volume approach. *Mech. Time-Depend. Mater.* **16**, 181–203 (2012)
- Diani, J., Liu, Y.P., Gall, K.: Finite strain 3D thermoviscoelastic constitutive model for shape memory polymers. *Polym. Eng. Sci.* **46**, 486–492 (2006)
- Diani, J., Gilormini, P., Frédy, C., Rousseau, I.: Predicting thermal shape memory of crosslinked polymer networks from linear viscoelasticity. *Int. J. Solids Struct.* **49**, 793–799 (2012)
- Doolittle, A.K.: Studies in Newtonian flow. II. The dependence of the viscosity of liquids on freespace. *J. Appl. Mech.* **22**, 1471–1475 (1951)
- Doolittle, A.K.: Studies on Newtonian flow. V. Further verification of the free-space viscosity equation. *J. Appl. Mech.* **28**, 901–905 (1957)
- Doolittle, A.K., Doolittle, D.B.: Studies in Newtonian flow. V. Further verification of the free-space viscosity equation. *J. Appl. Phys.* **28**, 901–905 (1957)
- Du, H., Zhang, J.: Solvent induced shape recovery of shape memory polymer based on chemically cross-linked poly(vinyl alcohol). *Soft Matter* **6**, 3370 (2010)
- Ferry, J.: *Viscoelastic Properties of Polymers*. Wiley, New York (1961), 482 pp.
- Francis, W.H., Lake, M.S., Schultz, M.R., Campbell, D., Dunn, M.L., Qi, H.J.: Elastic memory composite microbuckling mechanics: closed-form model with empirical correlation. In: 48th AIAA/ASME/ASCE/AHS/ASC Structures, Structural Dynamics, and Materials Conference, Honolulu, Hawaii (2007)
- Gall, K., Yakacki, C.M., Liu, Y.P., Shandas, R., Willett, N., Anseth, K.S.: Thermomechanics of the shape memory effect in polymers for biomedical applications. *J. Biomed. Mater. Res., Part A* **73A**, 339–348 (2005)
- Greaves, G.N., Greer, A.L., Lakes, R.S., Rouxel, T.: Poisson's ratio and modern materials. *Nat. Mater.* **10**, 823–837 (2011)
- He, J., Zhao, Y., Zhao, Y.: Photoinduced bending of a coumarin-containing supramolecular polymer. *Soft Matter* **5**, 308–310 (2009)
- Huang, W.M., Yang, B., An, L., Li, C., Chan, Y.S.: Water-driven programmable polyurethane shape memory polymer: demonstration and mechanism. *Appl. Phys. Lett.* **86**, 114105 (2005)
- Knauss, W.G., Emri, I.J.: Non-linear viscoelasticity based on free-volume consideration. *Comput. Struct.* **13**, 123–128 (1981)
- Knauss, W.G., Emri, I.: Volume change and the nonlinearly thermoviscoelastic constitution of polymers. *Polym. Eng. Sci.* **27**, 86–100 (1987)
- Lakes, R.S., Wineman, A.: On Poisson's ratio in linearly viscoelastic solids. *J. Elast.* **85**, 45–63 (2006)
- Lendlein, A., Kelch, S.: Shape-memory polymers. *Angew. Chem., Int. Ed. Engl.* **41**, 2035–2057 (2002)
- Lendlein, A., Kelch, S.: Shape-memory polymers as stimuli-sensitive implant materials. *Clin. Hemorheol. Microcirc.* **32**, 105–116 (2005)
- Lendlein, A., Langer, R.: Biodegradable, elastic shape-memory polymers for potential biomedical applications. *Science* **296**, 1673–1676 (2002)
- Lendlein, A., Jiang, H., Jünger, O., Langer, R.: Light-induced shape-memory polymers. *Nature* **434**, 879–882 (2005)
- Liu, C., Qin, H., Mather, P.T.: Review of progress in shape-memory polymers. *J. Mater. Chem.* **17**, 1543–1558 (2007)
- Lu, H., Knauss, W.G.: The role of dilatation in the nonlinearly viscoelastic behavior of PMMA under multi-axial stress states. *Mech. Time-Depend. Mater.* **2**, 307–334 (1999)
- Luo, X., Mather, P.T.: Triple-Shape Polymeric Composites (TSPCs). *Adv. Funct. Mater.* **20**, 2649–2656 (2010)
- Mather, P.T., Luo, X.F., Rousseau, I.A.: Shape memory polymer research. *Annu. Rev. Mater. Res.* **39**, 445–471 (2009)
- Mohr, R., Kratz, K., Weigel, T., Lucka-Gabor, M., Moneke, M., Lendlein, A.: Initiation of shape-memory effect by inductive heating of magnetic nanoparticles in thermoplastic polymers. *Proc. Natl. Acad. Sci. USA* **103**, 3540–3545 (2006)
- Nagata, M., Yamamoto, Y.: Photocurable shape-memory copolymers of epsilon-caprolactone and L-lactide. *Macromol. Chem. Phys.* **211**, 1826–1835 (2010)
- Nguyen, T., Jerryqi, H., Castro, F., Long, K.: A thermoviscoelastic model for amorphous shape memory polymers: incorporating structural and stress relaxation. *J. Mech. Phys. Solids* **56**, 2792–2814 (2008)

- Nguyen, T.D., Yakacki, C.M., Brahmabhatt, P.D., Chambers, M.L.: Modeling the relaxation mechanisms of amorphous shape memory polymers. *Adv. Mater.* **22**, 3411–3423 (2010)
- Odowd, N.P., Knauss, W.G.: Time-dependent large principal deformation of polymers. *J. Mech. Phys. Solids* **43**, 771–792 (1995)
- Ortega, A.M., Kasprzak, S.E., Yakacki, C.M., Diani, J., Greenberg, A.R., Gall, K.: Structure-property relationships in photopolymerizable polymer networks: effect of composition on the crosslinked structure and resulting thermomechanical properties of a (meth)acrylate-based system. *J. Appl. Polym. Sci.* **110**, 1559–1572 (2008)
- Popelar, C.F., Liechti, K.M.: A distortion-modified free volume theory for nonlinear viscoelastic behavior. *Mech. Time-Depend. Mater.* **7**, 89–141 (2003)
- Qi, H., Boyce, M.: Constitutive model for stretch-induced softening of the stress–stretch behavior of elastomeric materials. *J. Mech. Phys. Solids* **52**, 2187–2205 (2004)
- Rubinstein, M., Colby, R.H.: *Polymer Physics*. Oxford University Press, Oxford (2003)
- Schmidt, A.M.: Electromagnetic activation of shape memory polymer networks containing magnetic nanoparticles. *Macromol. Rapid Commun.* **27**, 1168–1172 (2006)
- Sherrod, P.H.: Nonlinear Regression Analysis Program, NLREG Version 5.0 (2000). Available from <http://www.nlreg.com/>
- Srivastava, V., Chester, S.A., Anand, L.: Thermally actuated shape-memory polymers: experiments, theory, and numerical simulations. *J. Mech. Phys. Solids* **58**, 1100–1124 (2010)
- Tschoegl, N.W., Knauss, W.G., Emri, I.: Poisson's ratio in linear viscoelasticity—a critical review. *Mech. Time-Depend. Mater.* **6**, 3–51 (2002)
- Westbrook, K.K., Kao, P.H., Castro, F., Ding, Y., Qi, H.J.: A 3D finite deformation constitutive model for amorphous shape memory polymers: a multi-branch modeling approach for nonequilibrium relaxation processes. *Mech. Mater.* **43**(12), 853–869 (2011)
- Williams, M.L., Landel, R.F., Ferry, J.D.: The temperature dependence of relaxation mechanisms in amorphous polymers and other glass-forming liquids. *J. Am. Chem. Soc.* **77**, 3701–3707 (1955)
- Xiao, R., Nguyen, T.D.: Modeling the solvent-induced shape-memory behavior of glassy polymers. *Soft Matter* **9**, 9455–9464 (2013)
- Xiao, R., Nguyen, T.D.: An effective temperature theory for the nonequilibrium behavior of amorphous polymers. *J. Mech. Phys. Solids* **82**, 62–81 (2015)
- Xie, T.: Tunable polymer multi-shape memory effect. *Nature* **464**, 267–270 (2010)
- Xie, T., Page, K.A., Eastman, S.A.: Strain-based temperature memory effect for nafion and its molecular origins. *Adv. Funct. Mater.* **21**, 2057–2066 (2011)
- Yakacki, C.M., Shandas, R., Lanning, C., Rech, B., Eckstein, A., Gall, K.: Unconstrained recovery characterization of shape-memory polymer networks for cardiovascular applications. *Biomaterials* **28**, 2255–2263 (2007)
- Yakacki, C.M., Satarkar, N.S., Gall, K., Likos, R., Hilt, J.Z.: Shape-memory polymer networks with Fe(3)O(4) nanoparticles for remote activation. *J. Appl. Polym. Sci.* **112**, 3166–3176 (2009)
- Yu, K., Qi, H.J.: Temperature memory effect in amorphous shape memory polymers. *Soft Matter* **10**, 9423–9432 (2014)
- Yu, K., Xie, T., Leng, J., Ding, Y., Qi, H.J.: Mechanisms of multi-shape memory effects and associated energy release in shape memory polymers. *Soft Matter* **8**, 5687–5695 (2012)
- Yu, K., Ge, Q., Qi, H.J.: Reduced time as a unified parameter determining fixity and free recovery of shape memory polymers. *Nat. Commun.* **5**, 3066 (2014a)
- Yu, K., McClung, A.J., Tandon, G.P., Baur, J.W., Qi, H.J.: A thermomechanical constitutive model for an epoxy based shape memory polymer and its parameter identifications. *Mech. Time-Depend. Mater.* **18**, 453–474 (2014b)
- Yu, K., Ritchie, A., Mao, Y., Dunn, M.L., Qi, H.J.: Controlled sequential shape changing components by 3D printing of shape memory polymer multimaterials. *Proc. IUTAM* **12**, 193–203 (2015)